On-chip cavity quantum phonodynamics with an acceptor qubit in silicon

Rusko Ruskov* and Charles Tahan†
Laboratory for Physical Sciences, 8050 Greenmead Drive, College Park, Maryland 20740, USA
(Received 13 November 2012; published 30 August 2013)

We describe a chip-based, solid-state analog of cavity-QED utilizing acoustic phonons instead of photons. We show how long-lived and tunable acceptor impurity states in silicon nanomechanical cavities can play the role of a matter nonlinearity for coherent phonons just as, e.g., the Josephson qubit plays in circuit QED. Both strong coupling (number of Rabi oscillations $\lesssim$100) and strong dispersive coupling (0.1–2 MHz) regimes can be reached in cavities in the 1–20-GHz range, enabling the control of single phonons, phonon-phonon interactions, dispersive phonon readout of the acceptor qubit, and compatibility with other optomechanical components such as phonon-photon translators. We predict explicit experimental signatures of the acceptor-cavity system.

DOI: 10.1103/PhysRevB.88.064308 PACS number(s): 63.20.kd, 03.67.Lx, 42.50.Pq, 73.21.Cd

I. INTRODUCTION

Circuit-QED has revolutionized the field of cavity-QED (cQED)[1–3] providing a stable platform for light-matter interaction in the microwave regime along with large couplings and solid-state integrability. Progress in the field has enabled applications such as single microwave photon sources[4] and quantum logic gates[3] on a chip. In an ideal crystal environment, phonons may play a role analogous to photons, though they propagate with the much slower speed of sound. That acoustic phonons can be quantum coherent has been explored in a number of architectures, allowing seminal experiments in optomechanical cooling,[5–10] trapping of phonons in phononic band-gap cavities,[6,10] photon translation via phonons,[11,12] and indirect qubit-phonon coupling.[13,14] What is missing to complete the analogy for phonons is a nonlinear element similar to an atom in cQED.

Such an element is possible, where an impurity transition in a crystal (e.g., two-levels of a Si donor) couples *directly* to confined phonons to form a hybridized state, which has been referred to as a phoniton (in analogy with a polariton).[15] The impurity-phonon interaction can be large due to a large deformation potential: $\langle\psi_{s'}|\hat{D}_{ij}|\psi_s\rangle \sim$ eV.[16] The previously proposed system[15] utilizing an umklapp *valley* transition of a donor in Si, however, requires very high frequencies (a few hundred GHz) and can be difficult to integrate with other phonon components. While other impurities such as in diamond[14] or in III–V semiconductors can offer smaller frequencies, a practical system in silicon would be highly desirable given recent demonstrations of high-Q cavities in silicon nanostructures,[10,17] silicon's investment in materials quality, and compatibility with CMOS technology and silicon photonics.

In this paper we propose an alternative quantum circuit element based on a single acceptor (such as B, Al, In) embedded in a patterned silicon nanomembrane, and driven by a long-wavelength phonon, $\lambda_{\text{phonon}} \gg a^*_{\text{acceptor}} \sim$ few nm, compatible with opto/mechanical components.[6,10] The acceptor two-level system (qubit), Fig. 1, has already been proposed for quantum computing[18] and is easily tunable in the 1–50-GHz range by external magnetic field and also by additional electric field or strain (allowing multiple qubit choices). We show how the acceptor-cavity system allows for both strong resonant coupling (where the qubit-phonon coupling g is greater than the loss mechanisms of the qubit and cavity, Γ_{qb}, κ_{cav}, respectively) and strong dispersive coupling, enabling the observability of a phonon vacuum Rabi splitting, and quantum nondemolition (QND) measurement of the cavity phonon number. Experimental signatures of the system are given, via magnetic field and temperature dependence (for $T \lesssim 1$ K), utilizing optical techniques.

II. ACCEPTOR QUBIT COUPLED TO CONFINED PHONONS

Hole valence bands in Si. Holes in Si require a richer physical picture[16,19] (compared to positrons in QED). The fourfold degeneracy [Fig. 1(a)] at the top of the valence band (neglecting heavy-light hole splitting) corresponds to propagation of particles of spin $J = 3/2$, reflecting the Γ_8 representation of cubic symmetry. Relatively large spin-orbit coupling implies also a twofold degenerate band (Γ_7 representation), split off by an energy gap $\Delta_{SO} \simeq 45$ meV.[16] For shallow acceptor centers in Si (e.g., B, Al, In, etc.) the ionization energy is $E_A \sim \Delta_{SO}$: thus, all valence bands will play a role in the acceptor states. Still, the lowest acceptor states remain fourfold degenerate since the acceptor spherical (Coulomb) potential does not change the cubic symmetry of the host crystal.[16]

A. Engineering the qubit levels

Two acceptor qubit arrangements are possible based on the lifting of the fourfold ground-state degeneracy via external fields. The related Hamiltonians are invariants of the cubic symmetry group $O_h = T_d \times I$ and time reversal[16,19] and are constructed from the momentum operator, $k_\alpha = \frac{1}{i}\frac{\partial}{\partial x_\alpha} + \frac{e}{c}A_\alpha$ (or the corresponding fields[16]) and the spin-3/2 operators $J_\alpha, \alpha = x,y,z$. The Zeeman type interaction is given by[16,19]

$$H_{\boldsymbol{H}} = \mu_B\left\{g'_1 \boldsymbol{J}\boldsymbol{H} + g'_2\left(J_x^3 H_x + \text{c.p.}\right)\right\}, \qquad (1)$$

where c.p. is cyclic permutation of x,y,z; the renormalized g values g'_1, g'_2 (μ_B is Bohr magneton), depending on the acceptor bound states, fulfill the relations $|g'_1| \approx 1$, $|g'_2| \ll |g'_1|$.[16,20,21] For a magnetic field $\boldsymbol{H}_z = (0,0,H_z)$ along the crystal [0,0,1] growth direction one can choose the lowest two Zeeman levels, $|\phi_1\rangle = |3/2\rangle$, $|\phi_2\rangle = |1/2\rangle$, as the qubit, which is the primary focus of this paper [Fig. 2(a)]. The qubit energy

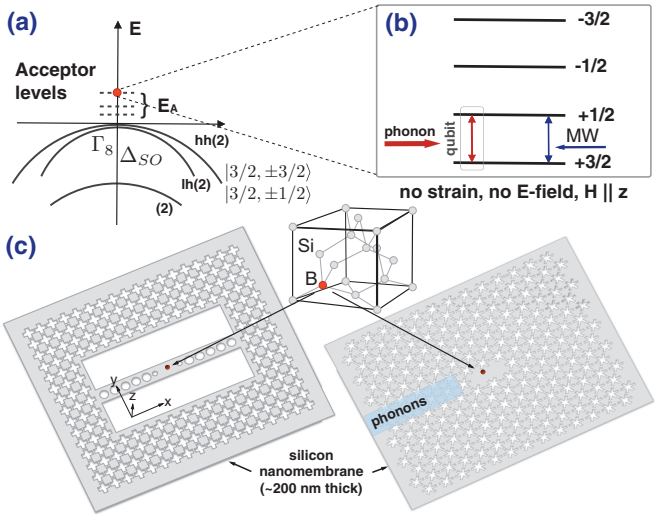

FIG. 1. (Color online) Acceptor:Si nanomechanical-cavity phoniton. (a) Hole valence bands in Si; fourfold degeneracy at the band top (and of lowest acceptor states) corresponds to particles of spin $J = 3/2$. (b) Ground-state splitting via external magnetic field along the [0,0,1] direction; level rearrangement is via additional strain. Strong coupling to a confined phonon mode and system manipulation via electric static/microwave fields is possible (see text). (c) Nanomechanical one-dimensional (1D) and 2D phonon band-gap cavities reminiscent of already fabricated high-Q cavities in a patterned Si membrane;[6,10] an on-chip phonon waveguide allows coupling to the acceptor-cavity phoniton system.

splitting $\delta E_H \simeq \mu_0 g_1' H$ is tunable in the range ≈1–40 GHz for $H = 0.1$–3 T. The qubic terms like $\sim g_2' J_x^3 H_x$ lift the level equidistancy: the outer splittings [Fig. 2(a)] are larger than the middle one by $\frac{3g_2'}{g_1'} \simeq 0.09$. For a field $\boldsymbol{H}$ tilted away from the crystal axis the qubit splitting is weakly angle dependent.

Alternatively, a second qubit arrangement involves mechanical stress in addition to the magnetic field. Stress lifts the ground-state degeneracy only partially: e.g., for stress along

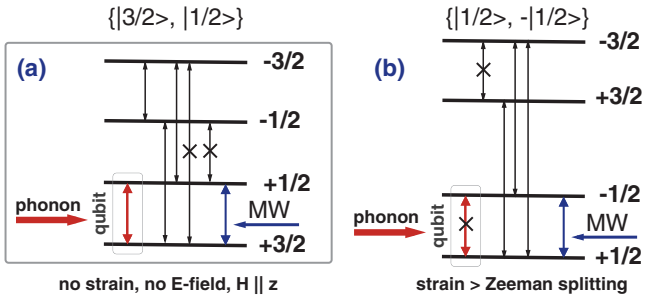

FIG. 2. (Color online) Two possible level arrangements as acceptor qubits. (a) Splitting due to magnetic field along a crystal direction (e.g., $\vec{H}||\hat{z}$). Allowed and forbidden phonon transitions and qubit phonon driving are shown. The qubit, $\{|1/2\rangle,|3/2\rangle\}$, is coupled strongly to a confined phonon, and can be manipulated via MWs. (b) Level splitting in presence of magnetic field and stress along the $\hat{z}$ direction, in the case of $\delta E_\varepsilon > \delta E_{\boldsymbol{H}}$. The alternate qubit, $\{|-1/2\rangle,|1/2\rangle\}$, is decoupled from phonons (to first order). The coupling and relaxation can be switched on via suitable electric field in the same direction (see text).

the crystal $\hat{z}$ direction [Fig. 1(c)], states $|\pm3/2\rangle$ and $|\pm1/2\rangle$ remain degenerate. Providing that the stress causes a splitting larger than the magnetic field splitting, the levels rearrange so that the lowest (qubit) levels will be $|\phi_1'\rangle = |-1/2\rangle$, $|\phi_2'\rangle = |1/2\rangle$, Fig. 2(b). This forms an alternate "phonon protected" qubit, decoupled from phonons to first order (the phonon coupling can be switched on via electric field; see below). The effect of strain, $\epsilon_{\alpha\beta}$, is described by the Bir-Pikus Hamiltonian:[16]

$$H_\epsilon = a' \,\mathrm{Tr}\,\epsilon_{\alpha\beta} + b'\,\epsilon_{xx}\,J_x^2 + \frac{d'}{\sqrt{3}}\,\epsilon_{xy}\,\{J_x J_y\}_+ + \text{c.p.} \qquad (2)$$

Experimentally,[20] the deformation potential constants for B:Si are $b' \simeq -1.42$ eV, $d' \simeq -3.7$ eV. Using H_ϵ we estimate a splitting of $\delta E_\varepsilon \approx 1$–10 GHz for external stress of 10^5–10^6 Pa. Such stress can be created in tensioned nanomembranes, improving also the mechanical Q factor.[9,22] A much larger stress ($\gtrsim 10^7$ Pa) due to a nearby (random) crystal defect,[23] or SiGe substrate results in a few hundred GHz splitting that would suppress the qubit-phonon coupling.

The role of the electric field. For a relatively weak electric field $\boldsymbol{E}$ the linear Stark effect is possible:

$$H_{\boldsymbol{E}} = \frac{p_E}{\sqrt{3}}(E_x\{J_y J_z\}_+ + E_y\{J_z J_x\}_+ + E_z\{J_x J_y\}_+), \qquad (3)$$

since an ion impurity actually reduces the cubic symmetry ($T_d \times I$) to T_d (and thus, there is no invariance under inversion).[16] The ground state splits to two doubly degenerate levels; however, the $H_{\boldsymbol{E}}$ does not commute with J_z for any direction of the field $\boldsymbol{E}$, leading to mixing of the Zeeman states. The latter can be useful to switch on/off the phonon coupling of the alternate qubit, $\{|-1/2\rangle,|1/2\rangle\}$ [Fig. 2(b)], provided the splitting $\delta E_{\boldsymbol{E}} = 2p_E|\boldsymbol{E}|$ is of the order of that due to stress, e.g., in the GHz range. The transition electric dipole moment p_E can be extracted from experiments: bulk dielectric absorption measurements[21] give $p_E \simeq 0.26$ D, with $D = 3.336 \times 10^{-30}$ C m being the Debye unit for e.d.m. (this is supported by single acceptor transport experiments[23]). Thus, a splitting of 1 GHz requires an electric field $|\boldsymbol{E}|_{1\text{Ghz}} \simeq 3.85 \times 10^5$ V/m, achievable in nanodevices.[24] Note, however, that increasing the field (splitting) exponentially decreases the qubit lifetime due to a (static field) acceptor ionization: for $\delta E = 1$ GHz the lifetime is $\tau_{\text{ion}} \approx 12$ s, while for $\simeq$1.26 GHz it is $\tau_{\text{ion}} \approx 12$ ms, etc.[24]

B. Coupling acceptor to a phonon mode

While there is no direct coupling of phonons to electronic spin, for the spin transitions of interest (e.g., $3/2 \to 1/2$) the spin states are actually "compound" states of p-like Bloch orbitals (spin 1) and electronic spin 1/2. Thus, coupling via deformation (a phonon) of the crystal is possible due to different orbital content of these states.

Here, we focus on the qubit $\{1 = |3/2\rangle, 2 = |1/2\rangle\}$ that does not require static strain. The coupling to a phonon mode is calculated by adding a quantized phonon field (see the Appendix) in addition to any classical field. We consider coupling to a plane-wave mode $\varepsilon_{\text{vac}}\,\boldsymbol{\xi}_{\boldsymbol{q}}^{(\sigma)}\,e^{-i\boldsymbol{q}\cdot\boldsymbol{r}}$ with polarization $\boldsymbol{\xi}_{\boldsymbol{q}}^{(\sigma)}$ (transverse, $\sigma = t_1, t_2$, or longitudinal, $\sigma = l$) and energy $\hbar v_\sigma q$, that proved to be a good estimation of coupling to modes

TABLE I. Key parameters for circuit QED (Ref. 26) (one-dimensional cavity), quantum dot (QD) QED (Ref. 27) vs the $\{|3/2\rangle,|1/2\rangle\}$ B:Si phoniton in a patterned Si membrane (of thickness $d = 200$ nm) phononic band-gap cavity; we show calculations for maximal coupling at frequencies of 1, 4, 8, and 14 GHz, for cavity volume $\mathcal{V} = d\lambda^2$ and $Q = 10^5$, using bulk T_1-limited linewidth Γ. The limiting frequency for strong dispersive coupling is reached at ≈21 GHz, when $\chi = \Gamma$; dressed state's resolution parameters are comparable to that in circuit QED.

Parameter	Symbol	Circuit QED	Quant. dot QED	B:Si (1 GHz)	B:Si (4 GHz)	B:Si (8 GHz)	B:Si (1 T)
Resonance freq.	$\omega_r/2\pi$	5.7 GHz	325 THz	1 GHz	4 GHz	8 GHz	14 GHz
Vac. Rabi freq.	$g/2\pi$	105 MHz	13.4 GHz	0.41 MHz	3.27 MHz	9.26 MHz	21.4 MHz
Cavity lifetime	$1/\kappa, Q$	0.64 μs, 10^4	5.5 ps, 1.2×10^4	15.9 μs, 10^5	4 μs	2 μs	1.14 μs
Qubit lifetime	$1/\Gamma$	84 ns	27 ps	386.5 μs	6 μs	0.75 μs	0.14 μs
Critical atom no.	$2\Gamma\kappa/g^2$	$\lesssim 8.6 \times 10^{-5}$	$\lesssim 1.87$	$\lesssim 4.9 \times 10^{-5}$	$\lesssim 2 \times 10^{-4}$	$\lesssim 3.9 \times 10^{-4}$	$\lesssim 6.9 \times 10^{-4}$
Crit. phonon no.	$\Gamma^2/2g^2$	$\lesssim 1.6 \times 10^{-4}$	$\lesssim 9.4 \times 10^{-2}$	$\lesssim 5.1 \times 10^{-7}$	$\lesssim 3.2 \times 10^{-5}$	$\lesssim 2.6 \times 10^{-4}$	$\lesssim 1.4 \times 10^{-3}$
No. Rabi flops	$2g/(\kappa+\Gamma)$	∼98	∼0.8	∼79	∼99	∼64	∼34
Cavity volume	$\mathcal{V}$	$10^{-6}\,\lambda^3$		$0.037\,\lambda^3$	$0.148\,\lambda^3$	$0.296\,\lambda^3$	$0.52\,\lambda^3$
Wavelength	λ	5.26 cm	921 nm	5400 nm	1350 nm	675 nm	385 nm
Dispersive coupling	$\chi \equiv g^2/\Delta$	17 MHz		0.04 MHz	0.33 MHz	0.93 MHz	2.14 MHz
Peaks' resolution	$2\chi/\Gamma$	∼6		∼199	∼25	∼9	∼4
No. of peaks	$2\chi/\kappa$	∼70		∼8	∼16	∼23	∼31

with realistic boundary conditions.[15] Moreover, the acceptor transition, unlike the {P/Li}:Si valley transition,[15,25] is less sensitive to the details of the confined phonon mode since the dipole approximation applies (as $\lambda_{\rm phonon} \gg a_B^*$; see Table I). The relevant matrix element is proportional to the "phonon vacuum field" strain, $\varepsilon_{\rm vac} \equiv (\frac{\hbar q}{2\rho\mathcal{V} v_\sigma})^{1/2}$; here ρ, $\mathcal{V}$, and v_σ are the mass density, mode volume, and sound velocity in Si. The coupling is obtained [for an acceptor placed at maximum *strain* of the cavity unlike in Ref. 15 where the (inter)valley transition requires placing the impurity at maximum *displacement*]:

$$g_\sigma^{3/2,1/2} = d' \left(\frac{\hbar\omega_{12}}{8\rho\hbar^2\mathcal{V}v_\sigma^2}\right)^{1/2} \begin{Bmatrix} \cos\theta, \sigma = t_1 \\ i\cos 2\theta, \sigma = t_2 \\ -i\sin 2\theta, \sigma = l \end{Bmatrix} e^{-i\varphi}, \qquad (4)$$

where the polar angles θ,φ of the wave vector $\boldsymbol{q}$ are with respect to $\boldsymbol{H}||\hat{z}$. Thus, the mode t_2 has a maximum along the phonon cavity ($\theta \approx \pi/2$); Fig. 1(c). An alternative is to have an in-plane magnetic field $\boldsymbol{H}_x$ along the crystal $[1,0,0]$ $\hat{x}$ direction (the latter is chosen to be along the phonon cavity): here, both modes t_1,t_2 (now at $\theta \approx 0$) are preferably coupled to the cavity. The maximal coupling $g_{\max,\sigma}^{3/2,1/2}$ scales as $\propto\sqrt{q/\mathcal{V}}$, as expected for a $(1s \to 1s)$ transition. For a cavity volume $\mathcal{V} \simeq d\lambda^2$ ($d = 200$ nm is the Si membrane thickness) we get coupling in the range $g/2\pi \simeq 0.4$–21 MHz for the frequencies of 1–14 GHz (Table I). The other allowed transition $|3/2\rangle \to |-1/2\rangle$ (at twice the qubit frequency) is well detuned, while the transitions $|3/2\rangle \to |-3/2\rangle$, $|1/2\rangle \to |-1/2\rangle$ are phonon forbidden [Fig. 2(a)].

Generally, when the in-plane magnetic field has some angle θ_0 with the cavity (crystal x axis), all transitions are allowed. Also, the qubit coupling to a preferably confined cavity phonon will change with the angle. As a qualitative example, consider a plane-wave transverse mode t_1 (or t_2) along the x axis: then, the coupling will change in the same way as in Eq. (4), with θ replaced by θ_0. This allows manipulation of the qubit-cavity coupling by in-plane rotation of the magnetic field.

For the alternate qubit, $\{|-1/2\rangle,|1/2\rangle\}$, the stress and magnetic field are parallel along the $\hat{z}$ direction [Figs. 1(c) and 2(b)]. Here the coupling is zero in the absence of electric field and can be switched on using nonzero electric field $\boldsymbol{E}_z$ in the same direction. The qubit-phonon coupling is given by the same Eq. (4) multiplied by a coupling factor, a function of the splitting ratios $r_h \equiv \frac{\delta E_H}{\delta E_\varepsilon}$, $r_e \equiv \frac{\delta E_E}{\delta E_\varepsilon}$: $f(r_h,r_e) = (\sqrt{z_+ z_-} - 1)/\sqrt{(1+z_+)(1+z_-)}$, with $z_\pm = [1 \pm \sqrt{(1 \mp r_h)^2 + r_e^2} \mp r_h]^2/r_e^2$. For a fixed magnetic field, $|f(r_h,r_e)| \to 0$ for small or large r_e. Thus, e.g., for $r_h = 0.5$–0.9 this factor reaches ≈0.25–0.65 for some optimal value of the electric-field splitting, $r_e \lesssim 1$, which allows strong qubit-cavity coupling.

These numbers show that there is an experimental strong-coupling "window" for the alternate qubit, $\{|-1/2\rangle,|1/2\rangle\}$, introduced above. For example, for a qubit (Zeeman) splitting of $\delta E_{\boldsymbol{H}} = 1$ GHz and a strain splitting $\delta E_\varepsilon = 1.43$ GHz (ratio of $r_h \equiv \frac{\delta E_H}{\delta E_\varepsilon} = 0.7$) the coupling factor reaches a maximal value of $f(r_h,r_e) \simeq 0.4$ for $\delta E_{\boldsymbol{E}} = 1$ GHz, i.e., $r_e = 0.7$. Analogously, for a qubit splitting of $\delta E_{\boldsymbol{H}} = 2$ GHz, this electric-field splitting leads to the same coupling factor of 0.4, giving a possibility for a strong acceptor-phonon coupling, and a relatively long (static field) ionization lifetime.

C. Strong coupling in an acceptor-phonon cavity system

Qubit relaxation rate. The qubit relaxation in the cavity is bounded at low temperatures by the bulk phonon spontaneous emission rate. For the $\{|3/2\rangle,|1/2\rangle\}$ qubit, at a magnetic field tilted by θ_0 from the crystal axis, we find

$$\Gamma_{3/2,1/2}(\theta_0) = \frac{(\hbar\omega_{12})^3}{20\pi\rho\hbar^4}\left\{d'^2(\cos^2 2\theta_0 + 1)\left[2/3v_l^5 + 1/v_t^5\right] + b'^2\,\sin^2 2\theta_0\left[2/v_l^5 + 3/v_t^5\right]\right\}. \qquad (5)$$

Here the contribution of longitudinal phonons is only a few percent (using speed of sound in Si: $v_l \simeq 1.7 \times v_t = 8.99 \times 10^3$ m s^{-1}). The results in Table I are for $\theta_0 = 0$. Note that the coupling in this case can be switched off (e.g., for a t_1 mode along the $\hat{x}$ direction, at $\theta_0 = \pi/2$) while the relaxation cannot.

For the alternate qubit, $\{|-1/2\rangle,|1/2\rangle\}$, the relaxation rate is $\Gamma_{1/2,1/2} = |f(r_h,r_e)|^2\,\Gamma_{3/2,1/2}(0)$, and can be switched on/off

simultaneously with the electric field, making it suppressed for zero electric field, as is the coupling.

The calculated relaxation times from Eq. (5) (Table I) are comparable to that in bulk Si at low B:Si doping (8×10^{12} cm^{-3} or 500 nm acceptor spacing), where $T_1^{\rm echo} \simeq 7.4$ μs and $T_2^{\rm echo} \simeq 2.6$ μs were measured[28] at 45 mK. Note that the single acceptor linewidth ($\sim 1/T^*_{2,\rm single}$) is the proper metric to compare g with, not the inhomogeneously broadened $1/T_2^*$ obtained from ensemble measurements.[29] While $T_2 = 2T_1$ for phonons alone, it may be limited by electric-dipole coupling to impurities,[18] magnetic hyperfine coupling to nearby nuclei ^{29}Si (expected to be small for holes), or charge noise (though here the acceptor is far away from surfaces or metal gates); both T_1, T_2 may improve for defect-free, low-doped,[20,21,30] and isotopically enriched samples;[29,31] T_1 may also improve in nanomembranes ($d \ll \lambda$) due to phase-space suppression (less available modes).

Phonon cavity loss. In the one-dimensional (1D)/2D-phononic band-gap Si nanomembranes considered here [Fig. 1(c)], the main cavity loss mechanism is due to (fabrication) symmetry-breaking effects, coupling the cavity mode to unconfined modes, and also due to cavity surface defects.[17] Bulk losses are negligible in the few-GHz range.[15,17] In this range the cavity Q factor, $Q \equiv \kappa/\omega$, can reach 10^4–10^5, or higher.[10,17]

Calculated rates in Table I show that *strong resonant coupling* is possible: $g_{12} \gg \Gamma_{12},\kappa$ in a wide frequency range, allowing ~30–100 Rabi flops. The low-frequency limit of 1 GHz is for $T \simeq 20$ mK, unless an active cavity cooling is performed[10] (see, however, Sec. III B below). A high-frequency limit of ~200 GHz is set by the different energy scaling of g and Γ. At high frequencies the Q factor will decrease; still, e.g., at 14 GHz, even $Q = 10^3$ leads to strong coupling.

D. Observing the phonon vacuum Rabi splitting

A suitable observable is the averaged phonon cavity field amplitude $|\langle \hat{b}_{\rm r} \rangle|$, which we have calculated, Figs. 3(a)–3(d), taking into account the first two excited dressed states (a "two-state approximation"[32]). In Fig. 3(a) we show the field amplitude $\langle \hat{b}_{\rm r} \rangle$ spectrum (ω_r is the cavity frequency) for $\omega_a = \omega_r = 8$ GHz vs external phonon driving frequency ω_d as two Rabi peaks at $\omega_r \pm g$. Figure 3(c) shows the "anticrossing picture" of the spectra at different acceptor detuning $\Delta_{\rm ar} = \omega_a - \omega_r$. Here the left resonance width and height are $\Gamma_L = \sin^2\Theta_0\Gamma + \cos^2\Theta_0\kappa$ and $\cos\Theta_0$, and for the right resonance one replaces $\sin\Theta_0 \leftrightarrow \cos\Theta_0$, with $\tan(2\Theta_0) = 2g/\Delta_{\rm ar}$. For large detuning, the surviving resonance acquires the dispersive shift $g^2/|\Delta_{\rm ar}|$, as expected.

Another option to observe the dressed resonance(s) is to sweep the qubit detuning (via the magnetic $\boldsymbol{H}$ field) while keeping the probe input frequency ω_d in resonance with the phonon cavity. As seen from Fig. 3(c), the field amplitude will exhibit a resonant dip, shown for different cavity frequencies, $\omega_r = 1,4,8,14$ GHz; Fig. 3(d). For large detuning the resonance is approximately a Lorentzian with a full width at half maximum, $\{\text{fwhm}\} \approx g^2/\kappa$ (a weak dependence on the qubit relaxation Γ is suppressed for strong coupling).

With increasing temperature the Rabi peak will be broadened[34] by the factor $1 + 2n_{\rm th}$ and the peak height will decrease by $2p_{\rm st} - 1$, where $p_{\rm st} = (1 + n_{\rm th})/(1 + 2n_{\rm th})$ is the ground-state occupation number. This is relevant for small thermal phonon number, $n_{\rm th} \equiv 1/(\exp[\hbar\omega_r/k_BT] - 1)$, at low T ($n_{\rm th} \lesssim 0.2$; see, e.g., Ref. 35). For $\omega_r/2\pi = 8$ GHz the Rabi peaks will be seen at 350 mK, but are negligible at 1 K [Fig. 3(b)]. At higher temperatures T, when $n_{\rm th} \gtrsim 1$, the lowest dressed states become saturated and in addition two broadened peaks will appear inside the Rabi doublet, Fig. 3(a) (not shown), roughly at frequencies $\delta\omega_d \simeq \pm g[\sqrt{n+1} - \sqrt{n}], n \approx n_{\rm th}$. These peaks will dominate over the Rabi peaks,[35] providing a signature of strong coupling even beyond 1 K.

III. MEASUREMENT VIA STANDARD TECHNIQUES

Ideally, one would probe the acceptor-cavity system with phonons. Direct phonon creation and detection should be possible via acoustic transducers.[36] As in a circuit QED experiment,[37] phonon correlations (antibunching) can be measured even without making single phonon counters. We note that other measurement approaches are possible via, e.g., hole transport[23,24] or scanning tunneling microscope (STM) probe spectroscopy.[38] However, here we consider an approach with single phonon sensitivity using a phonon-to-photon translator (PPT)[33] that can be realized on the same nanomembrane (with a simultaneous photon/phonon band gap; see Figs. 1(c) and 3(e).

A. Phonon-photon translator

Such a device is based on optomechanical nonlinearities that couple in the same band-gap cavity [Fig. 3(e)] two photon modes ($\hat{a}$,$\hat{a}_p$) and a phonon mode $\hat{b}$, via optomechanical coupling $h_{\rm om}$.[33] For photons in the near-infrared range ($\lambda_{\rm opt} \approx$ 1500 nm) the PPT allows one to couple a quantum optical input/output channel (of frequency $\omega/2\pi \simeq 200$ THz) to a phonon channel (with $\omega_d/2\pi \simeq 4$–8 GHz), and the coupling between the fields is enhanced by the auxiliary photon pump channel, pumping at the sideband resolved frequency $\omega_p = \omega - \omega_d - \Delta$ (at pump detuning $\Delta = 0$ it is at resonance with the red sideband of mode ω). The coherent nature of the photon-to-phonon translator is described by the effective beam-splitter type Hamiltonian:[39]

$$H_{\rm b-s} = -\Delta\hat{b}^\dagger\hat{b} + G_{\rm om}(\hat{a}^\dagger\hat{b} + \hat{a}\hat{b}^\dagger), \tag{6}$$

where $G_{\rm om} \propto h_{\rm om}E_0$ is the enhanced effective coupling, proportional to the pump field amplitude E_0. The weak-coupling regime, $G_{\rm om} < \kappa^{\rm opt}$ is needed to avoid total optical reflection, and optimal translation (close to 100%) takes place at a matching condition[33] $G_{\rm om} = \sqrt{\kappa^{\rm opt}\kappa^{\rm mech}}$ ($\kappa^{\rm opt}$, $\kappa^{\rm mech}$, are the couplings of the PPT to respective photon/phonon waveguides).

The PPT allows for optical techniques[7,10] to be applied to phononics components. We show in Fig. 3(e) an experimental schematic to measure the phonon cavity field $\langle \hat{b}_{\rm r} \rangle$ via a homodyne/heterodyne optical measurement.[34] To be able to scan around the mechanical resonance ω_r, one needs optical frequency resolution (at $\omega/2\pi \approx 200$ THz) better than the dressed state width, $(\Gamma + \kappa)/2\pi \approx 30$–$150$ kHz; Table I.

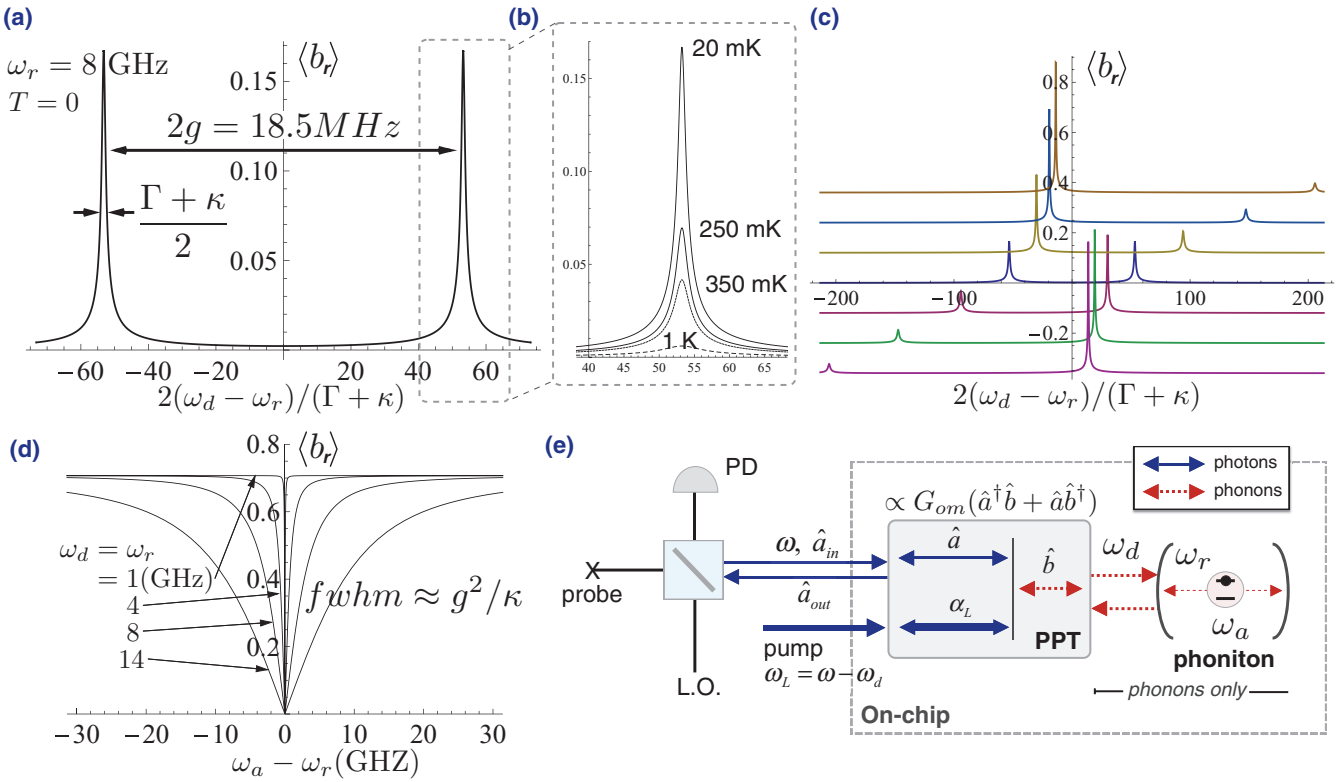

FIG. 3. (Color online) Intracavity field $\langle \hat{b}_r \rangle$ vs frequencies and temperature. (a) Rabi splitting in the strong resonant coupling regime as a function of a phonon signal sweep. (b) Rabi peaks vs temperature (approximate). At $n_{\rm th} \gtrsim 1$ broad peaks will appear inside the Rabi doublet (not shown) due to transitions to higher dressed states (see text). (c) "Anticrossing picture" at qubit-phonon cavity detuning, $\Delta_{\rm ar}$ (curves vertically shifted for clarity); for large positive detuning (upmost curve), the left resonance is dispersively shifted by $-g^2/\Delta_{\rm ar}$ while the right resonance is suppressed as $\sin\Theta_0$ (see text). (d) An alternative to determine the Rabi splitting: the absorption spectrum as a function of qubit detuning (via a magnetic field sweep). (e) Schematics of an optical homodyne/heterodyne experiment (see also Ref. 7) utilizing a phonon-to-photon translator (PPT).[33]

B. Acceptor "ionization" via optical photons

In the on-chip PPT implementation ideally no photon should enter the phoniton system, to avoid acceptor "ionization." However, since the photon-to-phonon translator is realized on the same Si nanomembrane (implying a simultaneous photonic/phononic band-gap structure) it is natural to ask how 200 THz photons may affect the qubit lifetime when or if they reach the acceptor. The corresponding photon energy of 0.82 eV is less than the indirect band gap in Si ($\Delta E_{\rm gap} = 1.1$ eV) and thus interband transitions are not possible. Thus, one considers an "ionization process" of a bound hole going to the continuous spectrum an analog of the ionization of an (anti)hydrogen atom (the corresponding cross section is thus rescaled). Correspondingly, one uses the rescaled values: a free hole mass $m_A \simeq 0.23\, m_e$ in Si, an effective Bohr radius $a_A^{\rm eff} = \frac{e^2 Z}{2[4\pi\varepsilon_0\varepsilon_r]E_A}$, with the acceptor ionization energy for B:Si, $E_A \approx 0.044$ eV, and screening factor $Z \simeq 1.4$. The total cross section is

$$\sigma_{\rm phot} = \frac{32\pi}{3} \frac{\hbar^6}{c\sqrt{2m_A}m_A^3\left[a_A^{\rm eff}\right]^5 E_f^{2.5}(E_f + E_A)} \frac{1}{[4\pi\varepsilon_0\varepsilon_r]}, \quad (7)$$

where $E_f = \hbar\omega - E_A$ is the final (free) hole energy, and $c = c_0/\sqrt{\varepsilon_r}$ is the speed of light in Si ($\varepsilon_r^{\rm Si} \simeq 11.9$). Since $E_A \ll E_f$, the total cross section is suppressed as $\propto 1/E_f^{3.5}$ (a final-state energy suppression). Given n_c photons in a cavity volume $\mathcal{V} \simeq d\lambda^2$ the acceptor lifetime is $\tau_{\rm phot} = 2\mathcal{V}/(n_c c\sigma_{\rm phot})$ for a maximum photon-acceptor overlap. Particularly, this may limit the ability to perform active photon (sideband) cooling of the phononic cavity (similar to Ref. 10) with an acceptor inside it. However, the estimated ionization cross section for B:Si is small, $\sigma_{\rm phot} \approx 8.6 \times 10^{-23}$ m^2: for ten photons in the cavity, at maximum photon-acceptor overlap, one gets an ionization lifetime of 12 μs. Notice that by placing the acceptor close to a node of the photon cavity, the ionization lifetime can increase considerably.

C. Strong dispersive coupling and phonon number states

A strong *dispersive coupling*, $\chi \equiv g^2/\Delta_{\rm ar}$, is reachable as per Table I. Since $\Delta_{ar} \geqslant 10g$ (dispersive regime) and $g^2/\Delta_{ar}\Gamma_{\rm relax} \geqslant 1$ (good resolution of phonon numbers), resolving the number states $|n\rangle$ in the phononic cavity would be possible. In the dispersive regime one can apply two tones (as in circuit-QED[26]): here, one tone is a *phonon* probe at ω_d, slightly detuned from the resonator [Fig. 3(e)]. The second (spectroscopic) tone, at ω_{sp}, is driving some of the dressed transitions around the acceptor frequency, at $\omega_a + (2n+1)\chi$,

via electric microwaves (MWs), similar to a manipulation of individual nitrogen-vacancy centers[14] (for B:Si a stronger MW coupling[21,28] is expected compared to nitrogen-vacancy centers). Thus, one could observe the *fine spectral structure* of the dressed cavity-acceptor system, predicted by Ref. 40 in a different context, by measuring the phonon (photon) reflection while sweeping the MW tone ω_{sp}.

IV. DISCUSSION AND APPLICATIONS

We have introduced a system that allows for on-chip manipulation of coherent acoustic phonons via coupling to acceptor qubit states in a nanomechanical cavity. Hybridization of the phonon-acceptor system and strong dispersive coupling are possible with comparable parameters to circuit-QED[26] and far surpassing semiconductor QD QED.[27] The cavity phoniton can be incorporated in more complex networks such as with phonon-photon interfaces to photonics,[10,33] and in arrays of phonitons for engineered many-body phonon devices.[15,41] From the perspective of qubits,[18,42] the isolated acceptor provides a potentially robust two-level system for quantum information processing. Our system offers an avenue for phonon dispersive readout of acceptor qubits and the potential for spin qubit-to-photon conversion in silicon.

APPENDIX: ACCEPTOR COUPLED TO A PHONON MODE

The impurity-acoustic phonon interaction,[16] $H^{\rm ac}_{\rm e,ph}(\boldsymbol{r}) = \sum_{ij} \hat{D}_{ij}\hat{\varepsilon}_{ij}(\boldsymbol{r})$, may lead to a strong-coupling regime ($g > \Gamma_{\rm qb}, \kappa_{\rm cav}$) even for cavity effective volume of few tens[15] of $\sim\lambda^3$. Qualitatively, the large coupling can be traced from the much smaller band gap ($\sim$ eV) in the "Si vacuum" as compared to QED ($\sim 10^6$ eV).

We account for the acceptor coupling to a quantized phonon field starting from the Bir-Pikus Hamiltonian, derived for a uniform classical strain field, Eq. (1) (see main text). For low-energy acoustic phonons the interaction Hamiltonian $\hat{H}_{\rm ph}$ has the same form with the strain operator $\hat{\varepsilon}_{ij}(\boldsymbol{r}) = \frac{1}{2}(\frac{\partial u_i}{\partial r_j} + \frac{\partial u_j}{\partial r_i})$ expressed via the quantized mechanical displacement:

$$\boldsymbol{u}(\boldsymbol{r}) = \sum_{\boldsymbol{q},\sigma} (\boldsymbol{u}_{\boldsymbol{q}\sigma}(\boldsymbol{r})\, b_{\boldsymbol{q}\sigma} + \boldsymbol{u}^*_{\boldsymbol{q}\sigma}(\boldsymbol{r})\, b^\dagger_{\boldsymbol{q}\sigma}). \tag{A1}$$

The mode normalization is

$$\int d^3\boldsymbol{r}\, \boldsymbol{u}^*_{\boldsymbol{q}\sigma}(\boldsymbol{r})\boldsymbol{u}_{\boldsymbol{q}\sigma}(\boldsymbol{r}) = \frac{\hbar}{2\rho\,\omega_{\boldsymbol{q}\sigma}}, \tag{A2}$$

so that $b^\dagger_{\boldsymbol{q}\sigma}$ creates a phonon in the mode $(\boldsymbol{q},\sigma)$ with energy $\hbar\omega_{\boldsymbol{q}\sigma}$ (ρ is the material mass density) in a mode volume $\mathcal{V}$. The vector $\boldsymbol{q}$ denotes a collective index of the discrete phonon mode defined via the phonon cavity boundary conditions and mode volume $\mathcal{V}$. Similar to cavity QED,[34] the phonon-acceptor coupling $\hbar g^{s's}_{\boldsymbol{q}\sigma} \equiv \langle s'; \boldsymbol{q}\sigma | H_{\rm ph} | s\rangle$ enters in a Jaynes-Cummings Hamiltonian (see, e.g., Ref. 15):

$$H_{\rm g} \approx \hbar g^{s's}_{\boldsymbol{q}\sigma}(\sigma^+_{s's} b_{\boldsymbol{q},\sigma} + \sigma^-_{s's} b^\dagger_{\boldsymbol{q},\sigma}), \tag{A3}$$

where we only retain the resonant cavity phonon, and $\sigma^+_{s's} \equiv |s'\rangle\langle s|$ refers to the relevant acceptor transition.

*ruskovr@gmail.com
†charlie@tahan.com

[1] H. J. Kimble, Phys. Scr. **T76**, 127 (1998).
[2] J. M. Raimond, M. Brune, and S. Haroche, Rev. Mod. Phys. **73**, 565 (2001).
[3] A. Blais, R. S. Huang, A. Wallraff, S. M. Girvin, and R. J. Schoelkopf, Phys. Rev. A **69**, 062320 (2004).
[4] A. A. Houck, D. I. Schuster, J. M. Gambetta, J. A. Schreier, B. R. Johnson, J. M. Chow, L. Frunzio, J. Majer, M. H. Devoret, S. M. Girvin, and R. J. Schoelkopf, Nature (London) **449**, 328 (2007).
[5] T. J. Kippenberg and K. J. Vahala, Science **321**, 1172 (2008).
[6] M. Eichenfield, J. Chan, R. M. Camacho, K. J. Vahala, and O. Painter, Nature (London) **462**, 78 (2009).
[7] S. Weis, R. Rivire, S. Deléglise, E. Gavartin, O. Arcizet, A. Schliesser, and T. J. Kippenberg, Science **330**, 1520 (2010).
[8] T. Rocheleau, R. Ndukum, C. Macklin, J. B. Hertzberg, A. A. Clerk, and K. C. Schwab, Nature (London) **463**, 72 (2010).
[9] J. D. Teufel, T. Donner, D. L. Li, J. W. Harlow, M. S. Allman, K. Cicak, A. J. Sirois, J. D. Whittaker, K. W. Lehnert, and R. W. Simmonds, Nature (London) **475**, 359 (2011).
[10] J. Chan, T. P. M. Alegre, A. H. Safavi-Naeini, J. T. Hill, A. Krause, S. Groeblacher, M. Aspelmeyer, and O. Painter, Nature (London) **478**, 89 (2011).
[11] V. Fiore, Y. Yang, M. C. Kuzyk, R. Barbour, L. Tian, and H. Wang, Phys. Rev. Lett. **107**, 133601 (2011).
[12] J. T. Hill, A. H. Safavi-Naeini, J. Chan, and O. Painter, Nat. Commun. **3**, 1196 (2012).
[13] A. D. O'Connell, M. Hofheinz, M. Ansmann, R. C. Bialczak, M. Lenander, E. Lucero, M. Neeley, D. Sank, H. Wang, M. Weides, J. Wenner, J. M. Martinis, and A. N. Cleland, Nature (London) **464**, 697 (2010).
[14] S. Kolkowitz, A. C. B. Jayich, Q. P. Unterreithmeier, S. D. Bennett, P. Rabl, J. G. E. Harris, and M. D. Lukin, Science **335**, 1603 (2012).
[15] Ö. O. Soykal, R. Ruskov, and C. Tahan, Phys. Rev. Lett. **107**, 235502 (2011).
[16] G. L. Bir and G. E. Pikus, *Symmetry and Strain-induced Effects in Semiconductors* (Keter, Jerusalem, 1974).
[17] J. Chan, A. H. Safavi-Naeini, J. Hill, S. Meenehan, and O. Painter, Appl. Phys. Lett. **101**, 081115 (2012).
[18] B. Golding and M. I. Dykman, arXiv:cond-mat/0309147.
[19] J. M. Luttinger, Phys. Rev. **102**, 1030 (1956).
[20] H. Neubrand, Phys. Status Solidi B **86**, 269 (1978).
[21] A. Köpf and K. Lassmann, Phys. Rev. Lett. **69**, 1580 (1992).
[22] S. S. Verbridge, D. F. Shapiro, H. G. Craighead, and J. M. Parpia, Nano Lett. **7**, 1728 (2007).
[23] L. E. Calvet, R. G. Wheeler, and M. A. Reed, Phys. Rev. Lett. **98**, 096805 (2007).
[24] G. D. J. Smit, S. Rogge, J. Caro, and T. M. Klapwijk, Phys. Rev. B **70**, 035206 (2004).
[25] V. N. Smelyanskiy, A. G. Petukhov, and V. V. Osipov, Phys. Rev. B **72**, 081304 (2005).

[26]D. I. Schuster, A. A. Houck, J. A. Schreier, A. Wallraff, J. M. Gambetta, A. Blais, L. Frunzio, J. Majer, B. Johnson, M. H. Devoret, S. M. Girvin, and R. J. Schoelkopf, Nature (London) **445**, 515 (2007).

[27]R. Bose, D. Sridharan, H. Kim, G. S. Solomon, and E. Waks, Phys. Rev. Lett. **108**, 227402 (2012).

[28]Y. P. Song and B. Golding, Europhys. Lett. **95**, 47004 (2011).

[29]H. Tezuka, A. R. Stegner, A. M. Tyryshkin, S. Shankar, M. L. W. Thewalt, S. A. Lyon, K. M. Itoh, and M. S. Brandt, Phys. Rev. B **81**, 161203(R) (2010).

[30]A. R. Stegner, H. Tezuka, H. Riemann, N. V. Abrosimov, P. Becker, H.-J. Pohl, M. L. W. Thewalt, K. M. Itoh, and M. S. Brandt, Appl. Phys. Lett. **99**, 032101 (2011).

[31]D. Karaiskaj, G. Kirczenow, M. L. W. Thewalt, R. Buczko, and M. Cardona, Phys. Rev. Lett. **90**, 016404 (2003).

[32]L. Tian and H. J. Carmichael, Phys. Rev. A **46**, R6801 (1992).

[33]A. H. Safavi-Naeini and O. Painter, New J. Phys. **13**, 013017 (2011).

[34]D. F. Walls and G. J. Milburn, *Quantum Optics* (Springer, Berlin, 2008).

[35]J. M. Fink, L. Steffen, P. Studer, L. S. Bishop, M. Baur, R. Bianchetti, D. Bozyigit, C. Lang, S. Filipp, P. J. Leek, and A. Wallraff, Phys. Rev. Lett. **105**, 163601 (2010).

[36]M. V. Gustafsson, P. V. Santos, G. Johansson, and P. Delsing, Nat. Phys. **8**, 338 (2012).

[37]D. Bozyigit, C. Lang, L. Steffen, J. M. Fink, C. Eichler, M. Baur, R. Bianchetti, P. J. Leek, S. Filipp, M. P. da Silva, A. Blais, and A. Wallraff, Nat. Phys. **7**, 154 (2011).

[38]S. Loth, K. von Bergmann, M. Ternes, A. F. Otte, C. P. Lutz, and A. J. Heinrich, Nat. Phys. **6**, 340 (2010).

[39]J. Zhang, K. Peng, and S. L. Braunstein, Phys. Rev. A **68**, 013808 (2003).

[40]M. I. Dykman and M. A. Krivoglaz, Sov. Phys. Solid State **29**, 210 (1987).

[41]P. Rabl, S. J. Kolkowitz, F. H. L. Koppens, J. G. E. Harris, P. Zoller, and M. D. Lukin, Nat. Phys. **6**, 602 (2010).

[42]J. J. Pla, K. Y. Tan, J. P. Dehollain, W. H. Lim, J. J. L. Morton, D. N. Jamieson, A. S. Dzurak, and A. Morello, Nature (London) **489**, 541 (2012).